Magnetic-field-induced charge localization in a high-mobility semiconductor superlattice

Petra Denk,* Martin Hartung, Martin Streibl, and Achim Wixforth
Sektion Physik der LMU, Geschwister Scholl Platz 1, D-80539 München, Germany

Kenneth L. Campman and Arthur C. Gossard
Materials Department, University of California, Santa Barbara, California 93196
(Received 28 October 1997; revised manuscript received 5 January 1998)

The charge distribution of mobile carriers in a high-mobility superlattice is investigated in magnetic fields parallel to the layers. Using a capacitance-voltage profiling technique we are able to directly probe the charge-density distribution as a function of spatial coordinate. With increasing in-plane magnetic field, we observe an increased localization in the potential wells of the superlattice. Using a simple model for the carrier distribution in the superlattice, we are able to calculate the magnetic-field dependence of the miniband structure in the sample. A tight-binding approach results in a quantitative description of the energy level separation as a function of the in-plane magnetic field. [S0163-1829(98)05920-7]

Ever since the first description of artificial superlattice (SL) structures by Esaki and Tsu,[1] the physics of strongly coupled electron systems in layered semiconductor structures has attracted more and more attention. Many different attempts to create such artificial SL's have been reported in the past. One elegant way to produce SL's with appreciably high mobilities is to use the method of remotely doped graded heterostructures, such as parabolic quantum wells (PQW's).[2] Here, the potential well is graded such that the engineered conduction and valence bands simulate the potential of a positive background charge without the need of dopants in the region of the quantum well. As compared to conventional semiconductor superlattices, the remote doping technique together with the graded band gap considerably enhances the electron mobility, mainly limited by size- and alloy-disorder scattering effects.[3] Shortly after the first realization of such PQW's, artificial superlattices have been introduced into them,[4,5] resulting in a very promising and interesting system for various physical observations. These include the observation of collective effects like magnetoroton resonances,[6] interminiband and intraminiband plasma excitations,[7] and the direct observation of the miniband structure in such SL's.[8]

On the other hand, the influence of strong magnetic fields on the properties of high-mobility semiconductor systems are of vivid interest for the last twenty years or so. Here, we investigate the effect of a strong in-plane magnetic field on the miniband structure of our high-mobility superlattices. An in-plane magnetic field, especially, induces interesting effects; for instance, the spatial direction of the electric (SL) potential and the one induced by the magnetic field coincide in this case. For very thick or very high barriers in the SL, there is no coupling between successive wells and the system behaves just like a set of isolated wells with the properties of quasi-two-dimensional electron systems. For thin barriers, however, the coupling between adjacent wells leads to a dispersion relation of a finite width in the SL direction (minibands) separated by a series of gaps (minigaps) as opposed to quantum wells with flat dispersion. In a magnetic field, the Lorentz force leads charged carriers to classically describe circular orbits with a cyclotron orbit radius R_N, depending on both the Landau quantum number N and the magnetic field B via

$$R_N^2 = (2N+1)l^2, \tag{1}$$

where $l = \sqrt{\hbar/eB} = 256\ \text{Å}/\sqrt{B}$ denotes the magnetic length. If the magnetic field is oriented parallel to the superlattice layers, the ratio of the magnetic length to the superlattice period will be an important parameter for the influence of the field on the SL properties.

Here, we would like to discuss the effect of such an in-plane magnetic field on the charge distribution in a superlattice structure. Experimentally, we approach the problem via a capacitance-voltage profiling technique that will be discussed in detail below. The sample used in our experiments is a 148-nm-wide, $Al_xGa_{1-x}As$ based PQW that has been grown by molecular-beam epitaxy using the digital alloy technique described elsewhere. To achieve the parabolic shape of the well, the aluminum content x in the active region has been varied between $x=0.01$ and $x=0.3$. In addition to the parabolic confining potential, a superlattice of $d=20$ nm period and $w=2$ nm barrier width has been grown into the well, the barrier height V_0 being determined by the Al content in the barrier material, in our case $V_0=75$ meV. A thin NiCr layer at the surface of the sample serves as a field effect electrode and small indium pellets at the corners of the sample as Ohmic contacts to the electron system in the well. Magnetotransport experiments reveal a carrier density of about $N_s=4\times10^{11}\ \text{cm}^{-2}$ for zero gate bias $V_g=0$.

A sketch of the sample and the resulting conduction- and valence-band structures including the charge distribution for flat-band conditions ($V_g=0$) is given in Fig. 1. The barriers in the SL are thin enough to allow for a substantial coupling between adjacent wells as indicated by a nonvanishing charge density in the barrier regions. The resulting charge distribution exhibits a modulation of period d as indicated in the figure. Application of a negative gate bias between the field effect electrode and the electron system pushes the

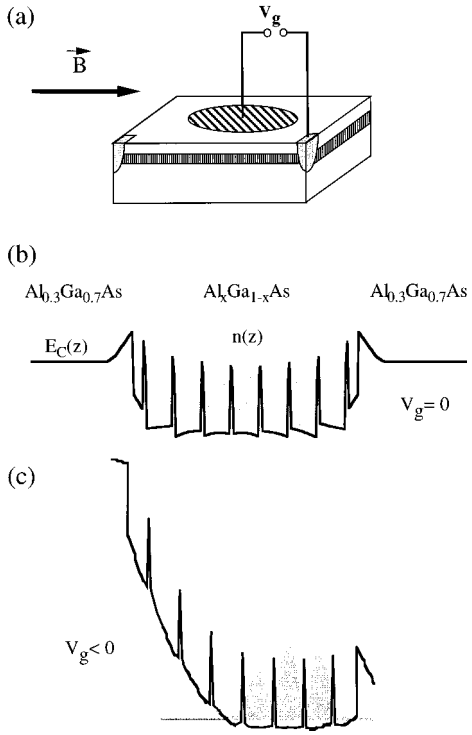

FIG. 1. (a) Sketch of the sample used for the CV profiling measurements described in the text. A gate bias between a field effect electrode (shaded circular structure on top) and the Ohmic contacts to the parabolic quantum well containing the SL (shaded areas parallel to the sample surface) is used to successively deplete one SL period after the other. (b,c) Schematic not to scale representation of the high-mobility superlattice structure used in our experiments. A wide parabolic quantum well has been modified by the insertion of an additional superlattice structure. The period of the superlattice is $d=20$ nm, the width of the barriers is $w=2$ nm. Remote doping of the structure leads to a carrier distribution as sketched in gray scale for flat-band condition (b) and a negative gate bias V_g (c).

center-of-mass of the charge distribution deeper towards the substrate and simultaneously slowly depletes the quantum well from free carriers. During this process, one SL well after another becomes successively depleted as well.

Capacitance-voltage (CV) profiling techniques have been shown before to be very valuable for the determination of the distribution of free charge within a given semiconductor system.[9] For the special case of a PQW, also the determination of the subband structure has become possible using a CV technique.[10,11] Caused by the finite thermodynamic density of states $D(E)$ of a quasi-two-dimensional electron system a change of the carrier density results in a considerable change in the chemical potential μ:

$$d\mu = e\,dV. \tag{2}$$

In other words, a change of the chemical potential μ is connected with a change of the induced charge Q by

$$dQ = AeD(E)d\mu = Ae^2D(E)dV. \tag{3}$$

Here, A denotes the area of the capacitor, i.e., the field effect electrode of our sample. As has been shown before,[10] the capacitance of a PQW as a function of the gate bias V_g can be basically divided into three contributions: (i) a geometrical capacitance C_{geo}, given by the thickness z_{geo} of the dielectric between the gate electrode and the electron system in the well,

$$C_{\mathrm{geo}} = \frac{\varepsilon_0\varepsilon_r A}{z_{\mathrm{geo}}}; \tag{4}$$

(ii) an additional term taking account of the fact that the center of mass of the charge distribution in a PQW (equivalent to the footpoint of the parabolic potential) shifts towards larger depths below the surface if a gate bias is applied,[10]

$$C(V_g) = \frac{\varepsilon_0\varepsilon_r A}{z(V_g)}; \tag{5}$$

(iii) a quantum mechanical contribution that originates from the above-mentioned dependence of the chemical potential μ on the density of states,

$$C_\mu = \frac{dQ}{dV} = Ae^2D(E). \tag{6}$$

Hence, the total capacitance of a PQW can be written as a series of these three contributions (4)–(6):

$$\frac{1}{C_{\mathrm{tot}}} = \frac{1}{C_{\mathrm{geo}}} + \frac{1}{C(V_g)} + \frac{1}{C_\mu}. \tag{7}$$

Term (6) has been used to evaluate the subband structure of a wide electron system in a PQW in the past. It has been shown that this contribution is very small as compared to those resulting from an inhomogeneous distribution of the charge in the well.[11]

Combining Eqs. (4)–(7) yields an analytic expression for the gate bias dependence of the coordinate- $z(V_g)$ in Eq. (5):

$$z(V_g) = \left(\frac{1}{C_{\mathrm{tot}}/A} - \frac{\pi\hbar^2}{e^2m^*}\right)\varepsilon_0\varepsilon_r - z_{\mathrm{geo}}. \tag{8}$$

To extract the apparent distribution of the charge as a function of the z coordinate, we use the well-known formula for CV profiling:[9]

$$n(z) = \frac{2}{e\varepsilon_0\varepsilon_r}\left[\frac{d}{dV}\left(\frac{1}{C^2}\right)\right]^{-1}. \tag{9}$$

Using $z(V_g)$ from Eq. (8), we now can easily convert a $C(V_g)$ measurement into an apparent $n(z)$ measurement, following our original aim. The true charge-density profile can then be evaluated from Eqs. (8) and (9) using a somewhat cumbersome procedure as described in Ref. 9. Here, however, we restrict ourselves to the determination of the apparent density profile $n(z)$, as it describes the reality well enough to elucidate the effect of the charge localization caused by the in-plane magnetic field.

A typical CV trace for the sample described here is shown in Fig. 2. The capacitance signal has been monitored using a standard lock-in technique at a frequency of about 90 Hz and a modulation amplitude of about 10 mV. The measurement has been performed at $T=4.2$ K with the sample mounted in the center of a superconducting solenoid providing in-plane magnetic fields up to $B=12$ T. With increasing negative gate bias the electron system in the PQW becomes slowly

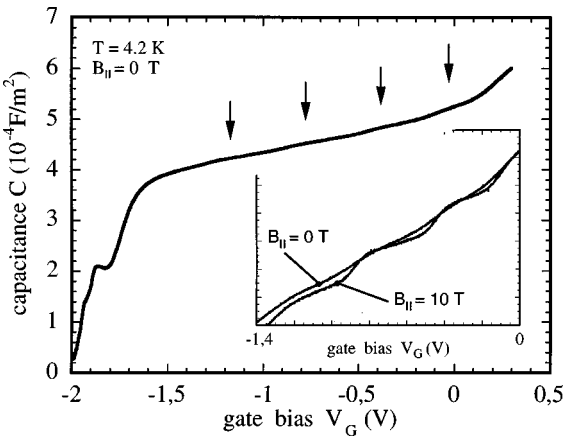

FIG. 2. Capacitance-voltage measurement for the high-mobility superlattice sample. As a function of increasing negative gate bias the quantum well containing the superlattice becomes depleted. This depletion is indicated by a slow overall decrease of the capacitance. At specific gate voltages, small steps in the CV trace (marked by arrows) indicate the subsequent depletion of individual potential wells of the superlattice. The inset shows how these steps evolve with increasing in-plane magnetic field.

depleted.[10] The shift of the center of the electronic wave functions towards larger depths below the surface is indicated by a small overall decrease of the CV signal until at about $V_g = -1.7$ V the complete depletion of the well sets in. Small steplike features (marked by arrows) on top of the CV signal indicate the subsequent depletion of adjacent wells in the superlattice. These steps evolve more clearly as the in-plane magnetic field is increased. The inset of the figure shows a comparison between a part of the CV trace at $B = 0$ T and the one taken at $B = 10$ T. Clearly, an increase in step height and in sharpness of the transition region between two steps is observed.

The result of the conversion of the CV traces into an apparent $n(z)$ dependence according to Eqs. (8,9) is shown in Fig. 3. Here, we plot the extracted charge density distribution $n(z)$ as a function of the real space coordinate z below the surface. The gray shaded boxes indicate the positions of the tunnel barriers in the superlattice, as taken from the growth protocol. As can be seen from the figure, four of the SL wells are occupied. With increase of the in-plane magnetic field B a pronounced localization of the charge in the wells between the barriers of the SL is observed. This is indicated by a decrease of the carrier density in the regions of the barriers, thus strongly reducing the coupling between the wells. At the same time, the charge density in the wells becomes larger as compared to the $B = 0$ case. This result is easily understood in terms of charge conservation.

To explain our experimental findings, we proceed using a simple harmonic approximation that allows for an analytic treatment of the effect of an in-plane magnetic field. The wave functions $\psi_i(z)$ in each individual well of the superlattice are approximated by harmonic oscillator wave functions, and the square wells in the superlattice are modeled by parabolic potential wells. This approximation will certainly not give the exact energy levels and the real density distribution but to first order it is very well suited to visualize the underlying physics. The charge distribution $n(z)$ that reflects the square of the total wave function $\langle \Psi | \Psi \rangle$ in the superlattice

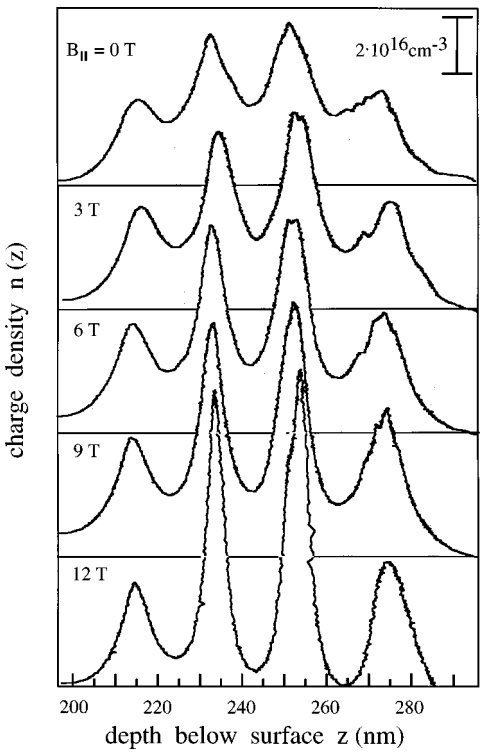

FIG. 3. Charge-density distribution $n(z)$ as extracted from the CV measurements at different in-plane magnetic fields. The gray shaded bars indicate the positions of the SL barriers as known from the growth. Four wells of the superlattice are occupied in our sample. With increasing in-plane field the charges become more and more localized in the potential wells, turning the strongly coupled superlattice band structure into that of a weakly coupled multiquantum well.

structure in this approximation is described by a sum of harmonic oscillator wave functions $\Psi_i(z)$, each of which being centered in one of the n occupied SL wells:

$$\Psi(z) = \sum_{i=-n/2}^{n/2} c_i \psi_i(z + id), \quad \psi_i(z) = \sqrt{\frac{\alpha}{\pi}} \exp\left(-\frac{\alpha z^2}{2}\right), \tag{10}$$

where $\alpha = m\omega_0/\hbar = 1.5 \times 10^{-4}$ Å^{-2} and the weighting factors c_i have been adjusted to properly describe the experimentally observed charge distribution $n(z)$ for $B = 0$ as shown in Fig. 3.

Using this ansatz, it is quite straightforward to include the effect of an in-plane magnetic field: An in-plane magnetic field adds a magnetic-field-induced potential of the form $V_B(z) = (m/2)\omega_C^2 z^2$ to the electrostatic (harmonic) potential $V_E(z) = (m/2)\omega_0^2 z^2$. Here, $\omega_c = eB/m$ is the cyclotron frequency. The frequency ω_0—as defined above—is the natural frequency of our harmonic test potential. The total confining potential is hence again parabolic and given by

$$V_{EB}(z) = \frac{m}{2}\omega_0^2 z^2 + \frac{m}{2}\omega_C^2 z^2$$

$$=: \frac{m}{2}\Omega^2 z^2 \quad \text{with} \quad \Omega^2 = \omega_0^2 + \omega_C^2. \tag{11}$$

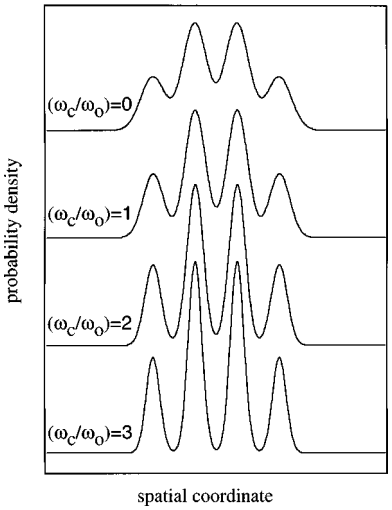

FIG. 4. Calculated charge distribution $n(z)$ using a simple harmonic approximation as described in the text. The magnetic field B is given in units of ω_c/ω_0. As in the experiment, with increasing in-plane magnetic field the charge becomes more and more localized in the individual wells of the superlattice.

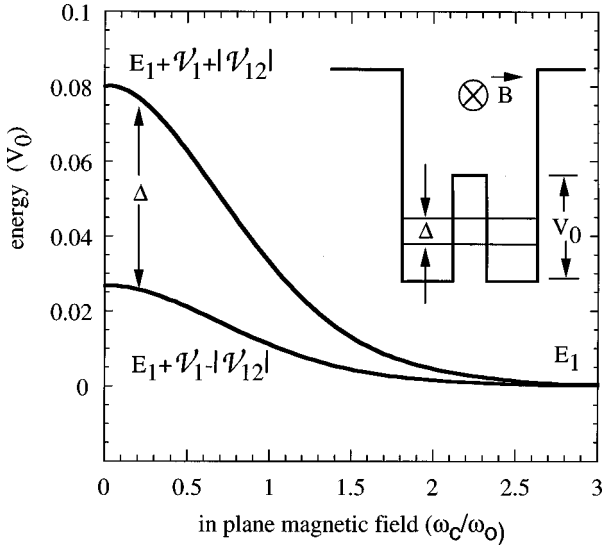

FIG. 5. Calculated level splitting Δ between the bonding and antibonding states of a coupled double quantum well. A simple tight binding approach together with an harmonic approximation as described in the text has been used. With increasing in-plane magnetic field, the level separation becomes smaller as the tunneling probability between adjacent wells is reduced. At the highest fields, the wells are completely decoupled as indicated by a well-defined ground-state energy E_1. The effect of the diamagnetic shift of this ground-state energy has been omitted in the calculation for the sake of clarity.

This result describes the well-known magnetoelectric hybridization of quantum well subbands in an in-plane magnetic field.[12] To model the effect of the in-plane field on the carrier distribution $n(z)$, we calculate $\Psi(z)$ form Eq. (10) using the hybrid potential of Eq. (11) and the hybrid frequency Ω for the local wave functions $\Psi_i(z)$.

The result is shown in Fig. 4. Here, we plot the calculated carrier distribution for a set of magnetic fields that is given in units of ω_c/ω_0. For our case, $\omega_c/\omega_0=1$ corresponds to an in-plane magnetic field of about 9 T. Clearly, the pronounced increase of the carrier localization is reproduced in the calculation. It is interesting to note that for such a strongly coupled superlattice as described here, very high in-plane magnetic fields of the order of 20 T are necessary to completely suppress the coupling between adjacent wells. This is consistent with our experimental findings: Even for the highest in-plane fields available to us ($B=12$ T), there is still a significant coupling observed, as indicated by a nonvanishing carrier density at the locations of the SL barriers (cf. lower panel in Fig. 3).

Using the above approximations for the in-plane field wave functions it is very instructive to calculate the behavior of the electronic level structure under the influence of the parallel magnetic field. At zero magnetic field, the wells in the superlattice are strongly coupled, resulting in a level splitting between the individual wells into ''bonding'' and ''antibonding'' states. For the finite superlattice discussed here, this results in the formation of a miniband with a finite number of discrete levels. As has been pointed out before, the in-plane field suppresses the tunnelling between adjacent wells in a superlattice, which results in a decoupling of the wells. As a measure for the strength of the tunneling-induced coupling we calculate the level separation using a tight-binding approach. Without losing the generality of the problem, we concentrate only on two neighboring wells. The self-energy matrix element $\mathcal{V}_1$ and the perturbation matrix element $\mathcal{V}_{12}$ between two adjacent wells in the superlattice are given by

$$\mathcal{V}_1=\langle\psi_1|V_2(z)|\psi_1\rangle=\langle\psi_2|V_1(z)|\psi_2\rangle,$$

$$\mathcal{V}_{12}=\langle\psi_1|V_2(z)|\psi_2\rangle=\langle\psi_2|V_1(z)|\psi_1\rangle, \tag{12}$$

where ψ_1 and ψ_2 represent the wave functions of an unperturbed single quantum well subjected to the in-plane field, and V_1 and V_2 the potential wells of the unperturbed and uncoupled problem. The energies of the bonding and antibonding levels are then given by

$$E=E_1+\mathcal{V}_1\pm|\mathcal{V}_{12}|, \tag{13}$$

where E_1 denotes the ground-state energy of the uncoupled wells. Under the influence of an in-plane field this ground-state energy is diamagnetically shifted towards higher energies, again described by the magnetoelectric hybridization mentioned above.[12] For the sake of clarity, however, we omit this shift in our calculations. The energetic splitting $|\mathcal{V}_{12}|$ between both levels—being proportional to the tunneling probability between adjacent wells—strongly decreases with increasing in-plane magnetic field. The result of this calculation is shown in Fig. 5. The magnetic field is again given in units of ω_c/ω_0, and the level splitting in natural units of the barrier height V_0 between the wells. As expected, we observe a strong decrease of the interwell tunneling and hence the coupling between the electron systems in adjacent wells. Our result describes exactly the same situation that one expects if the barrier height or width between two wells would be increased. One can thus state that an in-plane magnetic field effectively increases the width of a tunnel barrier between two quantum wells. This illustrative point of view has been discussed before by calculating the decreasing tunnel-

ing current through a barrier exposed to an in-plane field taking into account a magnetically ''curved trajectory'' in the barrier region.[13]

The magnetic-field-induced decoupling and the corresponding narrowing of the level splitting have also been observed in far-infrared studies and magnetotransport experiments on the same samples.[14,15] Here, we were able to directly measure the level splitting as a function of the in-plane field. The agreement with our simple estimate described here is very good.

In summary, we have demonstrated that an in-plane magnetic field strongly localizes the carriers in a semiconductor superlattice and hence reduces the coupling of adjacent wells. Using a capacitance-voltage profiling technique, we are able to directly monitor the charge distribution in the sample. Using a simple harmonic approximation and a tight-binding approach enables us to analytically calculate the magnetic-field-dependent bonding and antibonding level separation for our sample. The calculation is in excellent agreement with our experimental findings.

We gratefully acknowledge enlightening discussions with Th. Kraft, A. O. Govorov, and J. P. Kotthaus. We thank S. Manus, A. Kriele, W. Kurpas, and J. H. English for technical assistance. This work has been sponsored in part by the Deutsche Forschungsgemeinschaft and in part by the Air Force Office of Scientific Research. The Munich/Santa Barbara collaboration has been supported by a joint NSF/EEC grant, and by the BMBF via a Max-Planck-Forschungspreis.

*Present address: L2M, C.N.R.S., 196, Avenue Henri Ravera, 92225 Bagneux Cedex, France.

[1] L. Esaki and R. Tsu, IBM J. Res. Dev. **14**, 61 (1970).

[2] M. Sundaram, A. C. Gossard, J. H. English, and R. M. Westervelt, Superlattices Microstruct. **4**, 683 (1988); see also M. Shayegan, T. Sajoto, M. Santos, and C. Silvestre, Appl. Phys. Lett. **53**, 791 (1988).

[3] W. Walukiewicz, P. F. Hopkins, M. Sundaram, and A. C. Gossard, Phys. Rev. B **44**, 10 909 (1991).

[4] M. Sundaram, A. Wixforth, P. F. Hopkins, and A. C. Gossard, J. Appl. Phys. **72**, 1460 (1992).

[5] J. Jo, M. Santos, M. Shayegan, Y. W. Suen, L. W. Engel, and A-M. Lanzillotto, Appl. Phys. Lett. **57**, 2130 (1990).

[6] K. Karrai, X. Ying, H. D. Drew, M. Santos, M. Shayegan, S. R. E. Yang, and A. H. MacDonald, Phys. Rev. Lett. **67**, 3428 (1991).

[7] K. L. Campman, M. Sundaram, S. J. Allen, and A. C. Gossard, Superlattices Microstruct. **15**, 141 (1994).

[8] M. Streibl, R. J. Warburton, A. Wixforth, J. P. Kotthaus, K. Campman, and A. C. Gossard, in *The Physics of Semiconductors*, edited by M. Scheffler and R. Zimmermann (World Scientific, Singapore, 1996), Vol. 3, pp. 1739–1742.

[9] H. Kroemer, J. Vac. Sci. Technol. B **1**, 126 (1983); see also M. Sundaram, K. Ensslin, A. Wixforth, and A. C. Gossard, Superlattices Microstruct. **10**, 157 (1991); see also M. Sundaram and A. C. Gossard, J. Appl. Phys. **73**, 251 (1992).

[10] A. Wixforth, M. Sundaram, K. Ensslin, J. H. English, and A. C. Gossard, Appl. Phys. Lett. **56**, 454 (1990).

[11] A. J. Rimberg, S. Yang, J. Dempsey, J. H. Baskey, R. M. Westervelt, M. Sundaram, and A. C. Gossard, Appl. Phys. Lett. **64**, 390 (1992).

[12] W. Zawadzki, in *High Magnetic Fields in Semiconductor Physics II*, edited by G. Landwehr (Springer-Verlag, Berlin, 1988), p. 220.

[13] See, e.g., L. Eaves, K. W. H. Stevens, and F. W. Sheard, in *The Physics and Fabrication of Microstructures and Microdevices*, edited by M. J. Kelly and C. Weisbuch (Springer-Verlag, Berlin, 1986), pp. 343–51.

[14] M. Hartung, A. Wixforth, K. L. Campman, and A. C. Gossard, Superlattices Microstruct. **19**, 55 (1996).

[15] M. Hartung, P. Denk, M. Streibl, R. J. Warburton, A. Wixforth, K. Campman, P. F. Hopkins, and A. C. Gossard (unpublished).